# Integrated trajectory planning and control for obstacle avoidance manoeuvre using non-linear vehicle MP algorithm

Boyuan Li
*University of Wollongong*

Haiping Du
*University of Wollongong*, hdu@uow.edu.au

Weihua Li
*University of Wollongong*, weihuali@uow.edu.au

Bangji Zhang
*Hunan University*, bangjizhang@hnu.edu.cn

# Integrated trajectory planning and control for obstacle avoidance manoeuvre using non-linear vehicle MP algorithm

## Abstract

In the current literature, model-predictive (MP) algorithm is widely applied in autonomous vehicle trajectory planning and control but most of the current studies only apply the linear tyre model, which cannot accurately present the tyre non-linear characteristic. Furthermore, most of these studies separately consider the trajectory planning and trajectory control of the autonomous vehicle and few of them have integrated the trajectory planning and trajectory control together. To fill in above research gaps, this study proposes the integrated trajectory planning and trajectory control method using a non-linear vehicle MP algorithm. To fully utilise the advantages of four-wheel-independent-steering and four-wheel-independent-driving vehicle, the MP algorithm is proposed based on four-wheel dynamics model and non-linear Dugoff tyre model. This study also proposes the mathematical modelling of the static obstacle and dynamic obstacle for the obstacle avoidance manoeuvre of the autonomous vehicle. Finally, simulation results have been presented to show the effectiveness of the proposed control method.

## Disciplines

Engineering | Science and Technology Studies

## Publication Details

# Integrated trajectory planning and control for obstacle avoidance manoeuvre using nonlinear vehicle model-predictive algorithm

Boyuan Li [1,2], Haiping Du [2*], Weihua Li [3], Bangji Zhang[1]

[1] State Key Laboratory of Advanced Design and Manufacturing for Vehicle Body, Hunan University, Changsha 410082, China

[2] School of Electrical, Computer and Telecommunications Engineering, University of Wollongong, Wollongong, NSW 2522, Australia

[3] School of Mechanical, Material and Mechatronic Engineering, University of Wollongong, Wollongong, NSW 2522, Australia

[*]Corresponding author: hdu@uow.edu.au

**Abstract: In the current literature, model-predictive (MP) algorithm is widely applied in autonomous vehicle trajectory planning and control but most of current studies only apply the linear tyre model which cannot accurately present the tyre non-linear characteristic. Furthermore, most of these studies separately consider the trajectory planning and trajectory control of autonomous vehicle and few of them have integrated the trajectory planning and trajectory control together. To fill in above research gaps, this study proposes the integrated trajectory planning and trajectory control method using non-linear vehicle MP algorithm. In order to fully utilise the advantages of four-wheel-independent-steering (4WIS) and four-wheel-independent-driving (4WID) vehicle, the MP algorithm is proposed based on four wheel dynamics model and non-linear Dugoff tyre model. This study also proposes the mathematic modelling of the static obstacle and dynamic obstacle for the obstacle avoidance manoeuvre of the autonomous vehicle. Finally, simulation results have been presented to show the effectiveness of proposed control method.**

## 1. Introduction

The trajectory planning of the autonomous vehicle has become a popular research area due to the emergence of the intelligent transportation technology. Many of the studies in the current literature assumed the desired vehicle path was already known or the desired path has been planned by the off-line trajectory planner. Specifically, the autonomous vehicle was planned to follow the given trajectory which was assumed to be collision free and can be achieved by the vehicle [1] [2]. In [3], the combined lateral and longitudinal controller was used to follow the pre-calculated sigmoidal trajectories for the evasive manoeuvre, and a model predictive approach with a combined lateral and longitudinal dynamics model was also proposed in [4] to achieve the pre-calculated path. Rather than simply following a pre-defined path determined by an off-line planner, the practical application of autonomous vehicle requires to move autonomously to explore and determine the trajectory in real-time.

Model-predictive (MP) algorithm has been extensively applied in various control systems including industrial systems [5]. In the unmanned aerial vehicle control, MP algorithm was also applied to generate the desired safety path [6] [7]. In the area of on-road autonomous vehicle with more cluttered environment, the model-predictive algorithm was widely applied in the real-time trajectory planning and tracking control [8, 9, 10, 11]. Most of these studies only used the single point mass model and linear bicycle model. In [12], the desired vehicle trajectory could be planned by a single point mass model. In addition, a single track vehicle model was implemented as the representative of the actual vehicle dynamics performance and generated the feedback control inputs to achieve the trajectory control. The non-linear vehicle dynamics was not considered in the trajectory planner and controller. Although the computational efficiency is improved, the single mass model and linear bicycle model can hardly describe the actual vehicle non-linear dynamics. Thus, the planned trajectory sometimes cannot be achieved by the autonomous vehicle or the vehicle dynamics performance is

seriously compromised when following the planned trajectory. Yoon et al. proposed a MP algorithm to achieve the local path generation. This MP algorithm was based on 2-degree-of-freedom (2-DOF) non-linear bicycle model with the non-linear Magic formula tyre model and the steering angle and driving input of this lumped bicycle model were predicted [13]. Similarly, the 2-DOF bicycle model including the non-linear Magic Formula tyre model was applied in the MP algorithm to only predict the control input of steering rate and the velocity was assumed as the constant value in [14]. Although a non-linear tyre model is included in the trajectory planning in these studies, the applied two-wheel model can hardly present the non-linear dynamics performance of the innovative electric vehicle – four-wheel-independent-steering (4WIS) and four-wheel-independent-driving (4WID) electric vehicle equipped with four in-wheel motors. The individual wheel of the 4WIS-4WID electric vehicle can be independently steered and driven, and the non-linear four-wheel dynamics model is required to be included in the MP algorithm.

It was also argued that there is a compromise between the linear computational efficiency model and non-linear computational complex model when MP based algorithm was applied for the trajectory planning and control [15]. The linear simplified model is usually utilised as the high level path planner for the long prediction horizon, while the non-linear complex model is implemented as the low level path follower or trajectory tracking controller for the short prediction horizon. For example, a path planner chose a group of pre-defined paths from the lookup table in the high level and a 6-DOF non-linear bicycle model was applied for the trajectory tracking in the low level [16]. Similarly, a point-mass vehicle model was used to model the non-linear MP path planner and a more detailed vehicle dynamics model was applied for the trajectory tracking controller [17]. Few of the studies in the literature have considered integrating the trajectory planner and trajectory controller together based on MP algorithm. The computational efficiency can be improved due to the simplified and integrated control structure.

In this study, the non-linear Dugoff tyre model is integrated into the MP algorithm to predict the vehicle trajectory by considering the non-linear tyre characteristic. The four-wheel non-linear model is implemented in the MP algorithm, and the steering angle and driving or braking torque of individual wheel can be individually controlled and optimised in the real-time to fully utilise the advantage of 4WIS-4WID electric vehicle. In order to improve the computational efficiency of the non-linear MP algorithm, the non-linear vehicle model is implemented as the discrete-time model with fixed time step, and the steering angle and traction or brake torque can be optimised numerically. Instead of using the separated control structure of traditional trajectory planning and trajectory control method, this study proposes the MP algorithm based method which integrates the trajectory planner and trajectory controller together and the

computational efficiency can be improved by this integrated structure. The steering angle and traction or brake torque of individual wheel can be directly optimised and the local trajectory in real-time can be predicted simultaneously in this integrated MP based algorithm based on the real-time feedback vehicle states measured from the actual vehicle. The additional trajectory tracking controller is no longer required and the four predicted steering angles and four predicted driving or braking torques can be directly input into the 4WIS-4WID electric vehicle.

Furthermore, in the optimisation cost function in the proposed MP algorithm in this study, the predict trajectory is optimised by a potential field method to minimise the distance from the road centreline and maximise the distance from the road boundary and obstacle. The obstacle on the road can be classified as the static obstacle and dynamic obstacle and the proposed integrated method can predict the trajectory and control the vehicle to avoid the obstacle simultaneously in a fast and efficient manner.

This paper is organised as follows. The vehicle dynamics model of a 4WIS and 4WID electric vehicle is introduced in section 2. Then the MP based integrated trajectory planning and control algorithm is introduced. The bicycle model is first implemented in the proposed integrated control algorithm in section 3 and then the four-wheel model is implemented in section 4. In section 5, the mathematical modelling of the static obstacle and dynamic obstacle is built and incorporated into the MP control algorithm. Finally, simulation examples are used to validate the effectiveness of the proposed control method.

## 2. Vehicle dynamics model
### 2.1 Vehicle dynamics model

In this paper, a 4WIS and 4WID vehicle model is utilised to describe the dynamics motion of the electric vehicle with in-wheel steering and driving motors (Figure 1) [18] [19]. Based on this vehicle dynamics model, the steering angle and driving or braking torque of individual wheel can be predicted and optimised in real-time. The equations of motion of this model are described as follows:

$$m\dot{v}_x = mv_yr + \sum_{i=fl,fr,rl,rr} F_{xi}$$

(1a)

$$m\dot{v}_y = -mv_xr + \sum_{i=fl,fr,rl,rr} F_{yi}$$

(1b)

$$I_z\dot{r} = l_f(F_{yfl} + F_{yfr}) - l_r(F_{yrl} + F_{yrr}) + \frac{b_f}{2}(F_{xfl} - F_{xfr}) + \frac{b_r}{2}(F_{xrl} - F_{xrr})$$

$$\lambda_i = \frac{\mu F_{zi}(1-s_i)}{2\sqrt{C_s^2 s_i^2 + C_\alpha^2 \tan^2 \alpha_i}} \tag{3a}$$

$$f(\lambda_i) = \begin{cases} \lambda_i(2 - \lambda_i) & (\lambda_i < 1) \\ 1 & (\lambda_i > 1) \end{cases} \tag{3b}$$

$$F_{si} = \frac{C_\alpha \tan \alpha_i}{1-s_i} f(\lambda_i) \tag{3c}$$

$$F_{ti} = \frac{C_s s_i}{1-s_i} f(\lambda_i) \tag{3d}$$

According to equation (3), the Dugoff tyre model can be classified as two stages according to the defined value $\lambda$: when $\lambda > 1$, the tyre has not reached the sliding boundary point and when $\lambda < 1$, the tyre reaches the sliding boundary point and starts to slide away. The defined value $\lambda$ can clearly divide the whole tyre region into the linear tyre region and non-linear tyre region. $\mu$ is the tyre-road friction coefficient. $C_s$ is the longitudinal slip stiffness and $C_\alpha$ is the lateral cornering stiffness. The physical meaning of $C_s$ and $C_\alpha$ can be represented by the following equations [20]:

$$C_s = 2l^2 w k_x \tag{4a}$$

$$C_\alpha = 2l^2 w k_y \tag{4b}$$

where $l$ is the half-length of the contact patch and $w$ is the width of the contact patch. $k_x$ and $k_y$ are the tyre longitudinal deflection constant and lateral deflection constant related to the tyre property. $s_i$ is the longitudinal slip ratio, and $\alpha_i$ is the lateral slip angle. Longitudinal slip angle and can be calculated by the following equations:

$$s_i = \frac{R_\omega \omega_i - v_x}{R_\omega \omega_i} \quad \text{during acceleration} \tag{5a}$$

$$s_i = \frac{R_\omega \omega_i - v_x}{v_x} \quad \text{during braking} \tag{5b}$$

Lateral side-slip angle can be calculated as followings:

$$\alpha_{fl} = \delta_{fl} - \tan^{-1}\left(\frac{v_y + l_f r}{v_x - 0.5 b_f r}\right) \tag{6a}$$

$$\alpha_{fr} = \delta_{fr} - \tan^{-1}\left(\frac{v_y + l_f r}{v_x + 0.5 b_f r}\right) \tag{6b}$$

$$\alpha_{rl} = \delta_{rl} + \tan^{-1}\left(\frac{l_r r - v_y}{v_x - 0.5 b_r r}\right) \tag{6c}$$

$$\alpha_{rr} = \delta_{rr} + \tan^{-1}\left(\frac{l_r r - v_y}{v_x + 0.5 b_r r}\right) \tag{6d}$$

$F_{zi}$ is the vertical load of each wheel, which can be calculated as follows [21]:

$$F_{zfl} = \frac{m}{l_f + l_r}\left(\frac{1}{2} g l_r - \frac{1}{2}(\dot{v}_x - v_y r)h - \frac{l_r}{b_f}(\dot{v}_y + v_x r)h\right) \tag{7a}$$

---

(1c)

where $v_x, v_y, r$ are the vehicle longitudinal velocity, lateral velocity, and yaw rate, respectively. $i = fl, fr, rl, rr$, which represents the front left, front right, rear left and rear right wheel, respectively. $F_{xi}$ and $F_{yi}$ are longitudinal tyre force and lateral tyre force, respectively. $l_f$ and $l_r$ are the front and rear wheel base lengths, while $b_f$ and $b_r$ are the front and rear track widths. $I_z$ and $m$ are the moment of vehicle inertia in terms of yaw axis and vehicle mass.
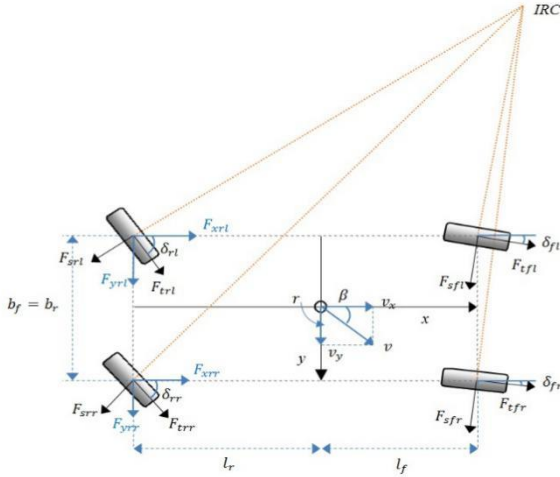


**Figure 1.** *4WIS-4WID vehicle dynamics model, where IRC represents the instantaneous centre of rotation.*

The tyre traction or brake force and side force are defined as $F_{ti}$ and $F_{si}$, respectively, which can be related to the longitudinal and the lateral tyre forces by the steering angle $\delta_i$ as follows:

$$F_{xi} = F_{ti} \cos \delta_i - F_{si} \sin \delta_i \tag{2a}$$

$$F_{yi} = F_{ti} \sin \delta_i + F_{si} \cos \delta_i \tag{2b}$$

where $\delta_i$ represents the steering angle of each vehicle wheel. It should be noted that all the steering angles mentioned in the paper indicate the steering angles of the vehicle wheels.

### 2.2 Vehicle tyre model

Although the non-linear Magic Formula tyre model is widely applied in the non-linear MP algorithm, the Magic Formula tyre model is mainly based on the curve fitting results of a particular group of experimental data and this kind of model is hard to describe the general physical meaning of tyre. The non-linear Dugoff tyre model, on the other hand, is the mathematical simplification of the analytical Fiala tyre model under some reasonable simplifying assumptions in the analysis of the tyre mechanics, which can accurately present the non-linear tyre property with simplified formulation [20]. The mathematic presentation of the non-linear Dugoff tyre model can be described as follows [20]:

3

$$F_{zfr} = \frac{m}{l_f+l_r}\left(\frac{1}{2}gl_r - \frac{1}{2}(\dot{v}_x - v_y r)h + \frac{l_r}{b_f}(\dot{v}_y + v_x r)h\right)$$

(7b)

$$F_{zrl} = \frac{m}{l_f+l_r}\left(\frac{1}{2}gl_f + \frac{1}{2}(\dot{v}_x - v_y r)h - \frac{l_f}{b_r}(\dot{v}_y + v_x r)h\right)$$

(7c)

$$F_{zrr} = \frac{m}{l_f+l_r}\left(\frac{1}{2}gl_f + \frac{1}{2}(\dot{v}_x - v_y r)h + \frac{l_f}{b_r}(\dot{v}_y + v_x r)h\right)$$

(7d)

where $h$ is the height of the vehicle CG above the ground, and $g$ is the acceleration of gravity.

### 2.3 Traction or brake dynamics model

Since one important feature of 4WIS-4WID electric vehicles is the ability to perform independent traction or brake motion for each wheel. The wheel rotation dynamics is described by the following equation:

$$I_\omega \dot{\omega}_i = -R_\omega F_{ti} + T_{di} \qquad \text{during traction} \qquad (8a)$$

$$I_\omega \dot{\omega}_i = -R_\omega F_{ti} - T_{bi} \qquad \text{during braking} \qquad (8b)$$

where $I_\omega$ is the wheel moment of inertia and $\omega_i$ is the angular velocity of each wheel. $R_\omega$ is the wheel radius and $T_{di}$ is the traction torque of each wheel and $T_{bi}$ is the brake torque of each wheel.

## 3. MP algorithm based on 2-DOF vehicle model

In this section, the proposed MP method based on 2-DOF model is presented to compare with the proposed MP algorithm based on four-wheel non-linear vehicle model to show the advantage of applied four-wheel model. The non-linear Dugoff tyre model is applied here to reflect the actual physical meaning and different types of the tyre. Based on the vehicle dynamics model (1), the two front wheels and two rear wheels can be lumped into one front wheel and one rear wheel:

$$m\dot{v}_x = mv_y r - F_{sf}\sin\delta_f + F_{tr}$$

(9a)

$$m\dot{v}_y = -mv_x r + F_{sf}\cos\delta_f + F_{sr}$$

(9b)

$$I_z \dot{r} = l_f F_{sf}\cos\delta_f - l_r F_{sr}$$

(9c)

where $F_{sf}$ and $F_{sr}$ are tyre side force of lumped front wheel and rear wheel and $F_{tr}$ is the tyre traction or brake force of rear wheel. It is assumed the 2-DOF vehicle model represents the front wheel steering and rear wheel driving vehicle. Thus, the rear wheel steering angle $\delta_r$ and traction or brake force of front wheel $F_{tf}$ can be assumed as zero.

Based on the Dugoff tyre model (3), the tyre forces can be calculated as follows:

$$F_{sf} = \frac{C_\alpha \tan\alpha_f}{1-s_f}f(\lambda_f)$$

(10a)

$$F_{sr} = \frac{C_\alpha \tan\alpha_r}{1-s_r}f(\lambda_r)$$

(10b)

$$F_{tr} = \frac{C_\alpha s_r}{1-s_r}f(\lambda_r)$$

(10c)

where $\alpha_f$ and $\alpha_r$ are side-slip angle of lumped front and left wheel; $s_f$ and $s_r$ are the slip ratio of lumped front and left wheel. $\alpha_f$ and $\alpha_r$ can be calculated as followings:

$$\alpha_f = \delta_f - \tan^{-1}\left(\frac{v_y + l_f r}{v_x}\right)$$

(11a)

$$\alpha_r = \tan^{-1}\left(\frac{l_r r - v_y}{v_x}\right)$$

(11b)

$\delta_f$ is the lumped value of front wheel steering angle. $\lambda_f$ is the lumped value of $\lambda_{fl}$ and $\lambda_{fr}$ and $\lambda_r$ is the lumped value of $\lambda_{rl}$ and $\lambda_{rr}$, which can be presented as follows:

$$\lambda_f = \frac{\mu F_{zf}(1-s_f)}{2\sqrt{C_s^2 s_f^2 + C_\alpha^2 \tan^2\alpha_f}}$$

(12a)

$$\lambda_r = \frac{\mu F_{zr}(1-s_r)}{2\sqrt{C_s^2 s_r^2 + C_\alpha^2 \tan^2\alpha_r}}$$

(12b)

where $F_{zf} = F_{zfl} + F_{zfr}$ and $F_{zr} = F_{zrl} + F_{zrr}$.

*Assumptions: It is assumed that the vehicle states of longitudinal velocity, lateral velocity and yaw rate can be successfully estimated and is available in the proposed MP algorithm. The vehicle vertical load and tyre-road friction coefficient are also assumed to be available. These assumptions are reasonable since a number of studies have successfully proposed the tyre-road friction estimator, lateral and longitudinal velocity estimator [22] [23] [24].*

Based on the 2 DOF tyre model (9)-(12), the cost function of MP optimisation algorithm can be presented as followings based on the attractive and repulsive potential fields suggested in [25]:

$$\min_{\delta_f, T_r} J_1 = a_1[(\hat{x}_a - X_d)^2 + (\hat{y}_a - Y_d)^2] +$$

$$b_1\left[\frac{1}{(\hat{y}_a - (Y_u - c_b))^2}\right] + b_2\left[\frac{1}{(\hat{y}_a - (Y_l + c_b))^2}\right]$$

(13a)

s.t. $\qquad -|\delta_{max}| \le \delta_f(k) \le |\delta_{max}| \qquad$ (13b)

$$-|T_{bmax}| \le T_r(k) \le |T_{dmax}| \qquad (13c)$$

4

$$-|\beta_{max}| \le \delta_f(k) - \tan^{-1}\left(\frac{v_y(k-1)+l_f r(k-1)}{v_x(k-1)}\right) \le |\beta_{max}|$$

(13d)

where $a_1$ is scaling factor of attractive potential and $b_1, b_2$ are scaling factors of repulsive potential. $a_1$ is related to the term of minimising the distance between the current vehicle position and road centerline. $b_1$ and $b_2$ are related to the term of maximising the distance between the current vehicle position and road boundaries. The values of these scaling factors can be adjusted according to the priority of different scenarios. The optimization variables are lumped front wheel steering angle $\delta_f(k)$ and lumped rear wheel traction or brake torque $T_r(k)$. $X_d$ and $Y_d$ are the longitudinal and lateral position of road centreline. $Y_u$ and $Y_l$ are lateral positions of road upper boundary and lower boundary. It is noted that the size of ego vehicle is also considered to make sure the edge of vehicle body (not the C.G. of vehicle body) will not collide with the upper or lower road boundary. The safety distance between the C.G. of ego vehicle and the road boundary can be determined by the following equation:

$$c_b = \max(l_f, l_r, b_f, b_r) + c_{bc} + c_{R_\omega}$$

(14)

where $\max(l_f, l_r, b_f, b_r)$ presents the geometry of vehicle body edge. $c_{R_\omega} = \frac{1}{2}R_\omega$ presents the circular safety gap extended from the vehicle body edge when considering the wheel turning and wheel side-slip. $c_{bc}$ is the constant value which presents the safety gap between the vehicle circular safety edge and road boundary. $\hat{x}_a$ and $\hat{y}_a$ are the predicted trajectory optimised by this MP algorithm, which can be presented by the following discrete dynamics model:

$$\hat{x}_a(k) = x_g(k-1) + \hat{v}_{xg}(k)\big(t(k) - t(k-1)\big) \quad (15a)$$

$$\hat{y}_a(k) = y_g(k-1) + \hat{v}_{yg}(k)\big(t(k) - t(k-1)\big) \quad (15b)$$

where $x_g(k-1)$ and $y_g(k-1)$ are feedback values of vehicle longitudinal and lateral position in the global coordinate system in the previous time step. $t_k$ is the time of current time step and $t_{k-1}$ is the time of previous time step. $\hat{v}_{xg}(k)$ and $\hat{v}_{yg}(k)$ are predicted vehicle longitudinal and lateral velocities in the global coordinate system in the current time step, which can be presented as following:

$$\hat{v}_{xg}(k) = \hat{v}_x(k)\cos\big(\hat{\varphi}(k)\big) - \hat{v}_y(k)\sin\big(\hat{\varphi}(k)\big) \quad (16a)$$

$$\hat{v}_{yg}(k) = \hat{v}_x(k)\sin\big(\hat{\varphi}(k)\big) + \hat{v}_y(k)\cos\big(\hat{\varphi}(k)\big) \quad (16b)$$

where $\hat{v}_x(k)$ and $\hat{v}_y(k)$ are predicted longitudinal and lateral velocity in the body-fixed coordinate system in the current time step and $\hat{\varphi}(k)$ is the predicted vehicle yaw angle in the current time step. According to equation (9), $\hat{v}_x(k)$, $\hat{v}_y(k)$ and $\hat{r}(k)$ can be predicted as followings:

$$
\begin{aligned}
\hat{v}_x(k) &= v_x(k-1) \\
&+ \Bigg(v_y(k-1)r(k-1) \\
&- \frac{\hat{F}_{sf}(k-1)\sin\delta_f(k-1) - \hat{F}_{tr}(k-1)}{m}\Bigg)\big(t(k) \\
&- t(k-1)\big)
\end{aligned}
$$

(17a)

$$
\begin{aligned}
\hat{v}_y(k) &= v_y(k-1) \\
&+ \Bigg(-v_x(k-1)r(k-1) \\
&+ \frac{\hat{F}_{sf}(k-1)\cos\delta_f(k-1) + \hat{F}_{sr}(k-1)}{m}\Bigg)\big(t(k) \\
&- t(k-1)\big)
\end{aligned}
$$

(17b)

$$
\begin{aligned}
\hat{r}(k) &= r(k-1) \\
&+ \Bigg(\frac{l_f\hat{F}_{sf}(k-1)\cos\delta_f(k-1) - l_r\hat{F}_{sr}(k-1)}{I_z}\Bigg)\big(t(k) \\
&- t(k-1)\big)
\end{aligned}
$$

(17c)

where $v_x(k-1)$, $v_y(k-1)$ and $r(k-1)$ are feedback values from actual vehicle in previous time step. $\hat{F}_{sf}(k-1)$, $\hat{F}_{sr}(k-1)$ and $\hat{F}_{tr}(k-1)$ are predicted tyre front wheel side force, rear wheel side force and rear wheel traction or brake force in the previous time step. Based on equations (10)(11), the tyre force $F_{sf}(k-1)$, $F_{sr}(k-1)$ and $F_{tr}(k-1)$ can be predicted as followings:

$$
\hat{F}_{sf}(k-1) = \begin{cases} \dfrac{C_\alpha \tan\big(\alpha_f(k-1)\big)}{1-s_f(k-1)} & \lambda_f > 1 \\[2ex] \dfrac{C_\alpha \tan\big(\alpha_f(k-1)\big)}{1-s_f(k-1)}\lambda_f\big(2-\lambda_f\big) & \lambda_f < 1 \end{cases}
$$

(18a)

$$
\hat{F}_{sr}(k-1) = \begin{cases} \dfrac{-C_\alpha \alpha_r(k-1)}{1-s_r(k-1)} & \lambda_r > 1 \\[2ex] \dfrac{-C_\alpha \alpha_r(k-1)}{1-s_r(k-1)}\lambda_r\big(2-\lambda_r\big) & \lambda_r < 1 \end{cases}
$$

(18b)

$$\hat{F}_{tr}(k-1) = \frac{T_r(k-1)}{R_\omega} \quad (18c)$$

where $\alpha_f(k-1) = \delta_f(k-1) - \tan^{-1}\left(\frac{v_y(k-1)+l_f r(k-1)}{v_x(k-1)}\right)$ and $\alpha_r(k-1) = -\frac{l_r r(k-1)-v_y(k-1)}{v_x(k-1)}$.

5

The lumped values of $\lambda_f$ and $\lambda_r$ can be calculated by equation (12). The longitudinal slip ratio $s_f(k-1)$ and $s_r(k-1)$ can be determined if the longitudinal velocity is assumed to be available. It is noted from (18) that the optimization variables of $\delta_f(k-1)$ and $T_r(k-1)$ are determined and can be input into the actual vehicle dynamics model.

The inequalities (13b) and (13c) show the constraints of the steering angle and driving or braking torque. For the electric vehicle, the practical limitation of the steering angle is considered between -90 degrees and 90 degrees ($\delta_{max} = 90$), which is larger than the traditional vehicle [26]. It has been also suggested [27] that the maximum driving torque of the single wheel $T_{dmax}$ is 100 N.m and the maximum regenerated brake torque $T_{bmax}$ is 80 N.m. Thus, it is assumed that the total maximum driving torque of lumped rear wheel of two DOF model $T_{dmax}$ is 200 N.m and the total braking torque $T_{bmax}$ is 160 N.m. In (13d), the maximum value of side-slip angle $\beta_{max}$ is constrained within a certain value to prevent the vehicle unstable motion. It is noted that only the side-slip angle of lumped front wheel is controllable, while the side slip angle of rear wheel is not controllable due to the front wheel steering characteristic. In the following section, the proposed optimisation algorithm based on four-wheel model can control the steering angle of individual wheel of the 4WIS-4WID electric vehicle to satisfy the side-slip angle constraint of individual wheel.

In this section, the vehicle trajectory in real-time can be predicted and optimised by equations (13)-(18) with the real-time feedback values from actual vehicle. The optimisation variables of steering angle and driving torque can be determined and input into the actual vehicle model.

## 4. MP algorithm based on four wheel non-linear vehicle model

The traditional two wheel model is hard to describe the dynamics performance and advantages of 4WIS-4WID electric vehicle. When the four wheel non-linear model is included in the MP algorithm, the individual wheel steering angle $\delta_i$ and traction or brake toque of individual wheel $T_i$ can be optimised to better achieve the desired trajectory. The cost function of the MP algorithm is similar to equation (13):

$$\min_{\delta_i, T_i} J_2 = a_1[(\hat{x}_a - X_d)^2 + (\hat{y}_a - Y_d)^2]$$
$$+ b_1 \left[ \frac{1}{(\hat{y}_a - (Y_u - c_b))^2} \right]$$
$$+ b_2 \left[ \frac{1}{(\hat{y}_a - (Y_l + c_b))^2} \right]$$

(19a)

s.t.
$$-|\delta_{max}| \leq \delta_i(k) \leq |\delta_{max}| \tag{19b}$$

$$-|T_{bmax}| \leq T_i(k) \leq |T_{dmax}| \tag{19c}$$

$$-|\beta_{max}| \leq \delta_{fl}(k) - \tan^{-1}\left(\frac{v_y(k-1)+l_f r(k-1)}{v_x(k-1)-0.5*b_f r(k-1)}\right) \leq |\beta_{max}| \tag{19d}$$

$$-|\beta_{max}| \leq \delta_{fr}(k) - \tan^{-1}\left(\frac{v_y(k-1)+l_f r(k-1)}{v_x(k-1)+0.5*b_f r(k-1)}\right) \leq |\beta_{max}| \tag{19e}$$

$$-|\beta_{max}| \leq \delta_{rl}(k) + \tan^{-1}\left(\frac{l_r r(k-1)-v_y(k-1)}{v_x(k-1)-0.5*b_r r(k-1)}\right) \leq |\beta_{max}| \tag{19f}$$

$$-|\beta_{max}| \leq \delta_{rr}(k) + \tan^{-1}\left(\frac{l_r r(k-1)-v_y(k-1)}{v_x(k-1)+0.5*b_r r(k-1)}\right) \leq |\beta_{max}| \tag{19g}$$

Similar to the bicycle model in the previous section, the vehicle predicted trajectory $\hat{x}_a$ and $\hat{y}_a$ in the current time step can be predicted and calculated from the vehicle velocity and yaw rate in the current time step based on equations (15)(16). The vehicle velocity and yaw rate can be predicted by the following equations based on non-linear four-wheel model (1)-(3):

$$\hat{X}_k = X_{k-1} + A_{k-1}(t(k) - t(k-1)) \tag{20}$$

where $\hat{X}_k$ is the predicted vehicle state $\hat{X}_k = \begin{vmatrix} \hat{v}_x(k) \\ \hat{v}_y(k) \\ \hat{r}(k) \end{vmatrix}$ and $X_{k-1}$ is the feedback vehicle state from the actual vehicle in the previous time step $X_{k-1} = \begin{vmatrix} v_x(k-1) \\ v_y(k-1) \\ r(k-1) \end{vmatrix}$ , $A_{k-1} = $

$$\begin{vmatrix} v_y(k-1)r(k-1) + \frac{\hat{F}_x(k-1)}{m} \\ -v_x(k-1)r(k-1) + \frac{\hat{F}_y(k-1)}{m} \\ \frac{\hat{M}(k-1)}{I_z} \end{vmatrix}.$$

It can be noticed in (20) that in order to predict the vehicle state in the current time step, the vehicle estimated total longitudinal tyre force $\hat{F}_x$, total lateral tyre force $\hat{F}_y(k-1)$ and yaw moment $\hat{M}(k-1)$ in the previous time step are required, which can be presented as follows:

$$\hat{F}_x(k-1) = \cos \boldsymbol{\delta}(k-1)\hat{\boldsymbol{F}}_t(k-1)$$
$$- \sin \boldsymbol{\delta}(k-1)\hat{\boldsymbol{F}}_s(k-1)$$

(21a)

$$\hat{F}_y(k-1) = \sin \boldsymbol{\delta}(k-1)\hat{\boldsymbol{F}}_t(k-1)$$
$$+ \cos \boldsymbol{\delta}(k-1)\hat{\boldsymbol{F}}_s(k-1)$$

(21b)

$$\hat{M}(k-1) = \boldsymbol{L_1}\hat{\boldsymbol{F}}_s(k-1) + \boldsymbol{L_2}\hat{\boldsymbol{F}}_t(k-1)$$

(21c)

6

where $\widehat{\boldsymbol{F}}_s(k-1) = \begin{bmatrix} \hat{F}_{sfl}(k-1) \\ \hat{F}_{sfr}(k-1) \\ \hat{F}_{srl}(k-1) \\ \hat{F}_{srr}(k-1) \end{bmatrix}$, $\widehat{\boldsymbol{F}}_t(k-1) =$

$\begin{bmatrix} \hat{F}_{tfl}(k-1) \\ \hat{F}_{tfr}(k-1) \\ \hat{F}_{trl}(k-1) \\ \hat{F}_{trr}(k-1) \end{bmatrix}$, $\cos\boldsymbol{\delta}\,(k-1) = \begin{bmatrix} \cos\delta_{fl}\,(k-1) \\ \cos\delta_{fr}\,(k-1) \\ \cos\delta_{rl}\,(k-1) \\ \cos\delta_{rr}\,(k-1) \end{bmatrix}^T$,

$\sin\boldsymbol{\delta}\,(k-1) = \begin{bmatrix} \sin\delta_{fl}\,(k-1) \\ \sin\delta_{fr}\,(k-1) \\ \sin\delta_{rl}\,(k-1) \\ \sin\delta_{rr}\,(k-1) \end{bmatrix}^T$ $\quad L_1 =$

$\begin{bmatrix} l_f\cos\delta_{fl}(k-1) - 0.5b_f\sin\delta_{fl}(k-1) \\ l_f\cos\delta_{fr}(k-1) + 0.5b_f\sin\delta_{fr}(k-1) \\ -l_r\cos\delta_{rl}(k-1) - 0.5b_r\sin\delta_{rl}(k-1) \\ -l_r\cos\delta_{rr}(k-1) + 0.5b_r\sin\delta_{rr}(k-1) \end{bmatrix}^T$

$L_2 = \begin{bmatrix} l_f\sin\delta_{fl}(k-1) + 0.5b_f\cos\delta_{fl}(k-1) \\ l_f\sin\delta_{fr}(k-1) - 0.5b_f\cos\delta_{fr}(k-1) \\ -l_r\sin\delta_{rl}(k-1) + 0.5b_r\cos\delta_{rl}(k-1) \\ -l_r\sin\delta_{rr}(k-1) - 0.5b_r\cos\delta_{rr}(k-1) \end{bmatrix}^T$

According to the non-linear Dugoff tyre model (3), $\hat{F}_{si}(k-1)$ and $\hat{F}_{ti}(k-1)$ can be determined as follows:

$$\hat{F}_{si}(k-1) = C_\alpha \tan\alpha_i(k-1) f(\lambda_i(k-1)) \tag{22a}$$

$$\hat{F}_{ti}(k-1) = \frac{T_i(k-1)}{R_\omega} \tag{22b}$$

where $\alpha_i(k-1)$ and $\lambda_i(k-1)$ can be determined by equations (6) and (3a).

Constraints (19b) and (19c) suggest the maximum steering angle and traction or brake torque of individual wheel. Constraints (19d)-(19g) show the limit value of side-slip angle of individual wheel.

The further stability analysis of the proposed MP algorithm based trajectory controller is required. It can be assumed that the error may exist in the predicted non-linear tyre force $F_{si}(k-1)$ and $F_{ti}(k-1)$ due to the parameter uncertainty (such as the estimation error of tyre-road friction coefficient) of the non-linear Dugoff tyre model:

$$\hat{F}_{si}(k-1) = F_{si}(k-1) + \Delta F_{si}(k-1) \tag{23a}$$

$$\hat{F}_{ti}(k-1) = F_{ti}(k-1) + \Delta F_{ti}(k-1) \tag{23b}$$

where $\hat{F}_{si}(k-1)$ and $\hat{F}_{ti}(k-1)$ show the predicted values of lateral tyre force and longitudinal tyre force of each wheel. $\Delta F_{si}(k-1)$ and $\Delta F_{ti}(k-1)$ present the tyre force prediction error caused by the tyre model parameter uncertainty, which is bounded.

$$|\Delta F_{si}(k-1)| \le C_1 \tag{24a}$$

$$|\Delta F_{ti}(k-1)| \le C_2 \tag{24b}$$

where $C_1$ and $C_2$ are constant values.

The total longitudinal tyre force, total lateral tyre force and total yaw moment considering the parameter uncertainty can be presented as follows:

$$\hat{F}_x(k-1) = F_x(k-1) + C_3 \tag{25a}$$

$$\hat{F}_y(k-1) = F_y(k-1) + C_4 \tag{25b}$$

$$\widehat{M}(k-1) = M(k-1) + C_5 \tag{25c}$$

where $C_3 = \sum_{i=fl,fr,rl,rr}\big(\Delta F_{ti}\cos\delta_i - \Delta F_{si}\sin\delta_i\big)$, $C_4 = \sum_{i=fl,fr,rl,rr}\big(\Delta F_{ti}\sin\delta_i + \Delta F_{si}\cos\delta_i\big)$ and $C_5 = \big[l_f\cos\delta_{fl}(k-1) - 0.5b_f\sin\delta_{fl}(k-1)\big]\Delta F_{sfl}(k-1) + \big[l_f\cos\delta_{fr}(k-1) + 0.5b_f\sin\delta_{fr}(k-1)\big]\Delta F_{sfr}(k-1) + \big[-l_r\cos\delta_{rl}(k-1) - 0.5b_r\sin\delta_{rl}(k-1)\big]\Delta F_{srl}(k-1) + \big[-l_r\cos\delta_{rr}(k-1) + 0.5b_r\sin\delta_{rr}(k-1)\big]\Delta F_{srr}(k-1) + \big[l_f\sin\delta_{fl}(k-1) + 0.5b_f\cos\delta_{fl}(k-1)\big]\Delta F_{tfl}(k-1) + \big[l_f\sin\delta_{fr}(k-1) - 0.5b_f\cos\delta_{fr}(k-1)\big]\Delta F_{tfr}(k-1) + \big[-l_r\sin\delta_{rl}(k-1) + 0.5b_r\cos\delta_{rl}(k-1)\big]\Delta F_{trl}(k-1) + \big[-l_r\sin\delta_{rr}(k-1) - 0.5b_r\cos\delta_{rr}(k-1)\big]\Delta F_{trr}(k-1)$. It is noted that the terms $C_3, C_4, C_5$ are bounded if the inequality (24) is satisfied. $F_x(k-1), F_y(k-1), M(k-1)$ are actual total longitudinal tyre force, total lateral tyre force and total yaw moment in $(k-1)$ time step. The predicted vehicle states can be presented as the following equation:

$$\begin{aligned}\hat{X}_k &= X_{k-1} \\ &+ \begin{vmatrix} v_y(k-1)r(k-1) + \dfrac{F_x(k-1) + C_3}{m} \\ -v_x(k-1)r(k-1) + \dfrac{F_y(k-1) + C_4}{m} \\ \dfrac{M(k-1) + C_5}{I_z} \end{vmatrix}(t(k) \\ &- t(k-1))\end{aligned} \tag{26}$$

Equation (26) suggests that the estimation error of vehicle states are bounded if $C_3, C_4, C_5$ are bounded. Therefore, if the error caused by tyre model parameter uncertainty is constrained within a certain value, the estimation errors of vehicle states are also bounded and the MP based controller is stable. It is noted that from equation (26) that the predicted vehicle states in current time step rely on actual feedback state values from previous time step. If the estimation error $C_3$, $C_4$ and $C_5$ are bounded, the estimation performance in the whole time range would not be greatly affected since the current estimated vehicle states can be real-time adjusted by the actual feedback values.

## 5. Definition and representation of static and dynamic obstacle

Collision avoidance is an important issue for the safety of the autonomous vehicle. In order to identify both the static and dynamic obstacles, several sensors are applied in the literature, such as Lidar [28], radar [29], stereo cameras [30] and the combination of those [31]. Alexander et al. can identify the potential collision with the dynamic obstacle only based on the image data from a monocular camera [32]. It is also argued in [33] that the technique of dedicated short-range communication (DSRC) has been applied in the vehicle industry by providing real-time and high-speed data links. Through the wireless network such as DSRC, the information of the nearby vehicles is available to the host vehicle for trajectory planning and control. Therefore, it can be assumed that the real-time position, velocity and heading angle of the obstacle nearby are assumed to be known in this study.

The on-road obstacles can be mainly classified as the static obstacle and dynamic obstacle. The static obstacle can be easily determined as the fixed coordinate values $(X_{ob}, Y_{ob})$ in the global coordinate system. It is noted that the size of ego vehicle and size of static obstacle should be considered in the obstacle avoidance control and a relative safety distance between the ego vehicle and obstacle should be maintained. This safety distance can be determined by the following equation:

$$c_i = c_b + c_{gi} \tag{27}$$

where $c_i$ $(i = 1,2, \ldots n)$ present the safety distances between vehicle and various obstacles. $c_{gi}$ presents the geometry size of obstacles.

The major disadvantage of proposed MPC based on attractive and repulsive potential field method is the obstacle trajectory can be generated only after the ego vehicle is too close to the obstacle and it is hard to maintain the safety distance. In order to tackle this issue and make sure the proposed MPC can achieve good obstacle avoidance performance, this study proposed a two-point repulsive potential to generate the real-time obstacle avoidance trajectory, which is presented in Figure 2. The two points refer to 'the boundary point' and 'obstacle point'. When the repulsive potential of the boundary point is considered, the MPC can generate the avoid trajectory in advance and keep the required safety distance between the ego vehicle and obstacle, which is advantageous over the method which only considers the repulsive potential of the obstacle point. The radius of the safety circle $R_{ci}$ can be determined as follows:
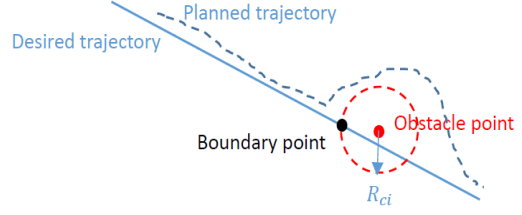
$$R_{ci} > c_i \tag{28}$$



**Figure 2.** *Diagram description of the two-point repulsive potential avoidance trajectory planning method for one particular static obstacle.*

When the static obstacle is considered, the cost function of MP algorithm (19) can be rewritten as followings:

$$
\begin{aligned}
\min_{\delta_i, T_i} J_3 \\
= a_1 [(\hat{x}_a - X_d)^2 + (\hat{y}_a - Y_d)^2] \\
+ b_1 \left[ \frac{1}{(\hat{y}_a - (Y_u - c_b))^2} \right] + b_2 \left[ \frac{1}{(\hat{y}_a - (Y_l + c_b))^2} \right] + \\
+ \sum_{i=1}^{n} \alpha_i b_{3i} \left[ \frac{1}{(\hat{x}_a - X_{bouni})^2 + (\hat{y}_a - Y_{bouni})^2} \right. \\
\left. + \frac{1}{(\hat{x}_a - X_{obi})^2 + (\hat{y}_a - Y_{obi})^2} \right]
\end{aligned}
$$

$$\tag{29}$$

where $(X_{bouni}, Y_{bouni})$ and $(X_{obi}, Y_{obi})$ are longitudinal and lateral coordinates of boundary point and obstacle point, respectively. The term $b_{3i}$ is suggested here to maximise the distance between the ego vehicle position and the positions of various static obstacles. The other actuator constraints and vehicle dynamics constraints in (19b)-(19g) are still applied in cost function as (29b)-(29g). $\alpha_i$ can be considered as the trigger factor of the obstacle avoidance term $b_{3i}$. If the vehicle is far away from the static obstacle, the obstacle avoidance term $b_{3i}$ is not triggered ($\alpha_i = 0$). Otherwise, if the vehicle is close to the obstacle point, the obstacle avoidance term is triggered ($\alpha_i = 1$). The mathematical presentation of this condition can be shown as follows:

$$\text{If} \quad (\hat{x}_a - X_{obi})^2 + (\hat{y}_a - Y_{obi})^2 \geq c_{ti}^2, \alpha_i = 0 \tag{30a}$$

$$\text{If} \quad (\hat{x}_a - X_{obi})^2 + (\hat{y}_a - Y_{obi})^2 < c_{ti}^2, \alpha_i = 1 \tag{30b}$$

where $c_{ti}$ is the trigger distance between the ego vehicle position and obstacle position, which can be determined by the following equation:

$$c_{ti} = v_x T_t \tag{31}$$

where $T_t$ is the trigger time in advanced of the collision happen.

On the other hand, the situation when the moving obstacles are considered is discussed here. The single point mass model is usually applied to describe the moving obstacle, which can be presented as followings:

$$\dot{X}_{ob} = V_{ob} \cos \theta \qquad (32a)$$

$$\dot{Y}_{ob} = V_{ob} \sin \theta \qquad (32b)$$

where $a_{xob} = \dot{V}_{ob} \cdot V_{ob}$, $a_{xob}$ and $\theta$ are the longitudinal velocity, longitudinal acceleration and heading angle of moving obstacles, respectively. When the real-time position of the obstacle is already available in (32), the cost function of the MP algorithm when the moving obstacle is considered can be presented the same as the cost function in equation (29).

## 6. Simulation results

In this section, three sets of simulations are carried out by the software of Matlab Simulink to verify the advantageous of the proposed integrated trajectory planner and controller based on the MP algorithm and 4WIS-4WID vehicle model over the MP algorithm based on two-wheel model. In addition, in order to clearly show the improved performance of proposed method, the simulation results of traditional two-level trajectory tracking method [25] is also presented. In the simulation implementation of this section, the optimisation solver 'active-set' is applied to obtain the optimisation results, which is more time-efficiency than the default solver 'interior-point'.The vehicle parameters are listed in Table 1 and the scaling factors in the optimisation algorithm of all the compared methods are presented in Table 2.

**Table 1.** Vehicle parameters used in simulations [19].

| | | |
|---|---|---|
| $m$ | Mass | 1298.9 kg |
| $l_f$ | Distance of c.g. from the front axle | 1 m |
| $l_r$ | Distance of c.g. from the rear axle | 1.454 m |
| $b_f$ | Front track width | 1.436 m |
| $b_r$ | Rear track width | 1.436 m |
| $C_s$ | Longitudinal stiffness of the tyre | 50000 N/unit slip |
| $I_z$ | Vehicle moment of inertial about yaw axle | 1627 kgm² |
| $R_\omega$ | Wheel radius | 0.35 m |
| $I_\omega$ | Wheel moment of inertial | 2.1 kgm² |
| $\varepsilon_r$ | Road adhesion reduction factor | 0.015 s/m |
| $C_\alpha$ | Cornering stiffness of the tyre | 30000 N/unit slip |
| $h$ | height of the vehicle centre of gravity | 0.533 m |
| $c_{bc}$ | Safety gap | 0.25 m |
| $T_t$ | Trigger time in advance of the collision | 2.5 s |
| $b_{max}$ | Maximum lateral side-slip angle | 0.2 rad |

**Table 2.** Scaling factors in the optimization algorithm in each set of simulations.

| Simulation | Algorithm | $a_1$ | $a_2$ | $b_1$ | $b_2$ | $b_{31}$ | $b_{32}$ |
|---|---|---|---|---|---|---|---|
| 1 | Two-level method | N/A | N/A | N/A | N/A | N/A | N/A |
| | Four-wheel MPC | 1000 | 1000 | 0 | 0 | 0 | 0 |
| | Two-wheel MPC | 1000 | 1000 | 0 | 0 | 0 | 0 |
| 2 | Two-level method | 100 | 75 | 5000 | 5000 | 5750 | 5750 |
| | Four-wheel MPC | 100 | 75 | 5000 | 5000 | 5750 | 5750 |
| | Two-wheel MPC | 100 | 75 | 5000 | 5000 | 5750 | 5750 |
| 3 | Two-level method | 100 | 75 | 5000 | 5000 | 5750 | N/A |
| | Four-wheel MPC | 100 | 75 | 5000 | 5000 | 5750 | N/A |
| | Two-wheel MPC | 100 | 75 | 5000 | 5000 | 5750 | N/A |

In the first set of simulations, the autonomous vehicle is implementing a simple lane change task on the highway. The road centreline and road boundary are depicted in Figure 3. It is noted that this road boundary has considered the safety

gap and is constrained between $[Y_u - c_b, Y_l + c_b]$. The initial velocity of the autonomous vehicle is 10 m/s and the tyre–road friction coefficient is assumed as 0.9. Furthermore, the actual trajectories of the 4WIS-4WID autonomous vehicle controlled by the proposed MP algorithm based on the four-wheel model, the MP algorithm based on two-wheel model and traditional two-level method are compared and shown in Figure 3. It is noted that for the traditional two-level method, the desired trajectory is assumed to be planned and known already and the two-level trajectory tracking controller is implemented to achieve the desired trajectory. The trajectories of all the three methods can accurately follow the road centreline. Figure 4(a) shows the vehicle yaw rate response of all the three methods and the proposed MP method based on four-wheel model shows more stable yaw rate response and less yaw angle change rate compared with other methods. Figure 4(a) also suggest that the actual trajectory and yaw rate responses of the MP method based on two-wheel model and traditional two-level method are oscillating abruptly and the reason behind this should be discussed further. For the traditional two-level method, the reason behind this is the desired trajectory is pre-defined and the trajectory cannot be smoothly optimised in real-time. For the two-wheel model based MP method, the MP optimisation algorithm cannot fully utilise the characteristic of 4WIS-4WID vehicle and the yaw stability performance of the controlled vehicle is compromised. However, in Figure 4(b), the proposed MP algorithm based on four-wheel model has larger side-slip angle response compared to two-wheel model method and traditional two-level method. The main reason of this is that the excessive tyre force is applied in order to minimise the yaw angle change rate. The generation of additional tyre force causes the increase of the side-slip angle.

In the second set of simulations, the autonomous vehicle is still implementing the single lane change task with the same boundary condition in Figure 3. However, two static obstacles are assumed to locate in the road centre line with the coordinates values of (105, -2) and (185, -4) in the global coordinate system. The size of these two obstacles are assumed as $c_{g1} = c_{g2} = 0.5\ m$. The initial velocity and tyre-road friction coefficient are the same as the first set of simulation, but the vehicle will deaccelerate after 5 seconds to test the robustness control performance of proposed MPC. It is noted that instead of following the pre-defined path in the first set of simulation, the traditional two-level method applies the potential field method [25] to generate the obstacle avoidance trajectory. The proposed four-wheel MPC and two-wheel MPC methods both apply the two-point repulsive potential method to generate the avoidance trajectory. The blue point indicates the boundary point and black point is the obstacle point. Figure 5 presents the actual vehicle trajectory of the proposed method and traditional methods. It is indicated that the traditional two-level method can just avoid the obstacle point but the safety distance between the ego vehicle and obstacle cannot be maintained. The proposed MP algorithm based on the four-wheel model

and two-wheel model can successfully generate the avoidance trajectory and also maintain the safety distance.
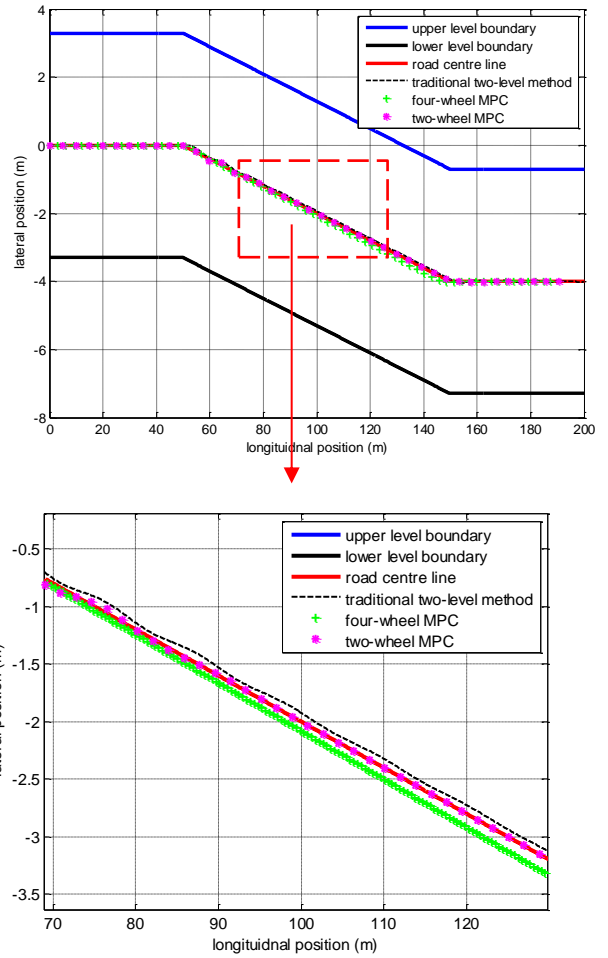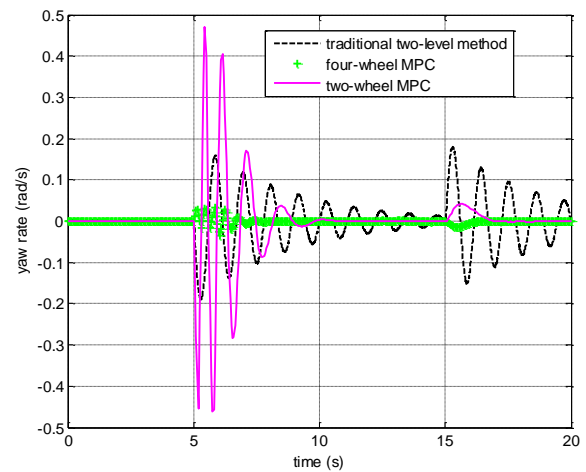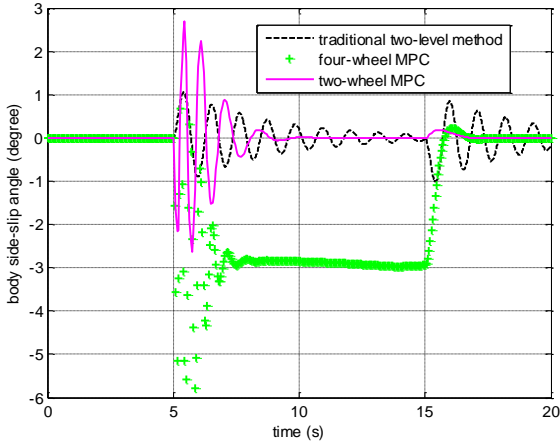




**Figure 3.** *Vehicle desired and actual trajectory in the first set of simulations.*



(a)

(b)

***Figure 4.*** *Vehicle dynamics response in the first set of simulations.*
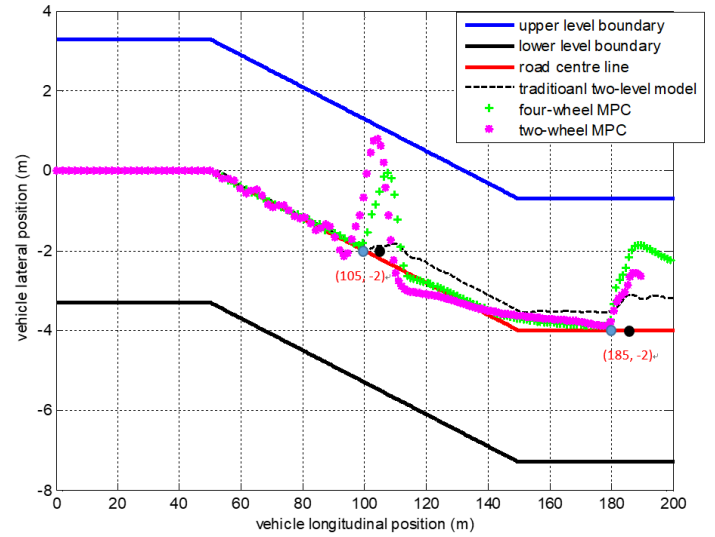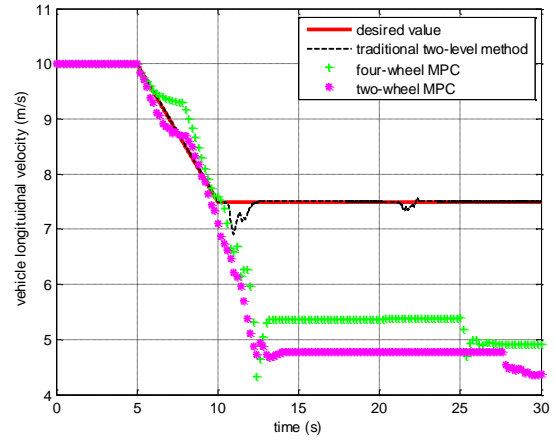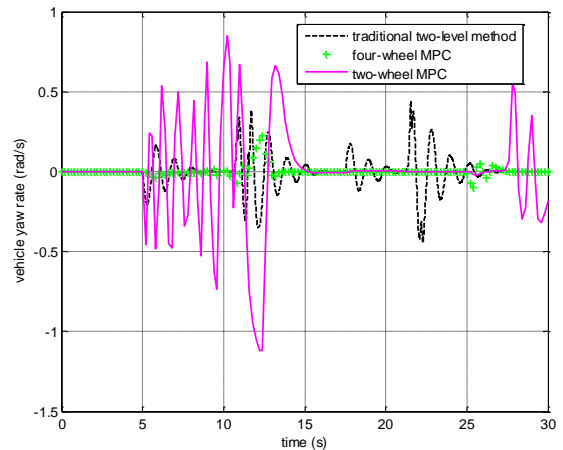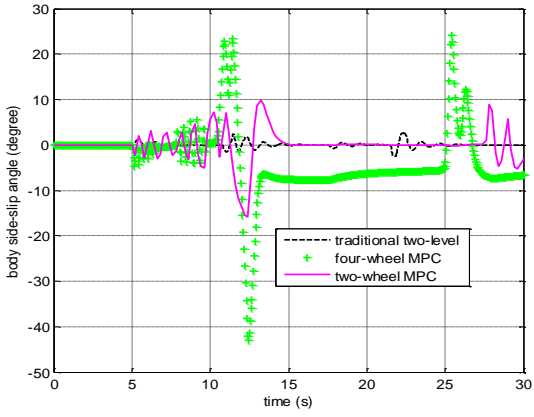
**(a)** yaw rate **(b)** body side-slip angle



***Figure 5.*** *Vehicle desired and actual trajectory in the second set of simulations.*

Figure 6(a) suggests the longitudinal velocity response of all the three methods and it can be observed the vehicle is deaccelerating after 5 seconds. Figure 6(b) shows the yaw rate response of all the three methods. The proposed four-wheel model based method has smooth yaw rate response compared with the two-wheel model method when the obstacle avoidance manoeuvre is implemented. Figure 6(c) shows that the body side-slip angle of four-wheel model based method is larger than the two-wheel model based method since the additional force is applied to better avoid the obstacle with smaller yaw rate. The traditional two-level method generates the avoidance trajectory with smaller lateral displacement and consequently the response of yaw rate and body side-slip angle are smaller than MPC methods. Figures 7(a) and 7(b) show the steering angle response of the front left wheel and rear right wheel, while Figures 7(c) and 7(d) suggest the side-slip angle response of front left wheel and rear right wheel. The steering angle or side-slip angle of front right wheel is similar to the front left wheel, and the steering angle of rear left wheel is similar to the rear right wheel, which are not presented in Figure 7. It can be seen form Figure 7 that all the proposed methods satisfy both the constraints of individual wheel steering angle and side-slip angle.
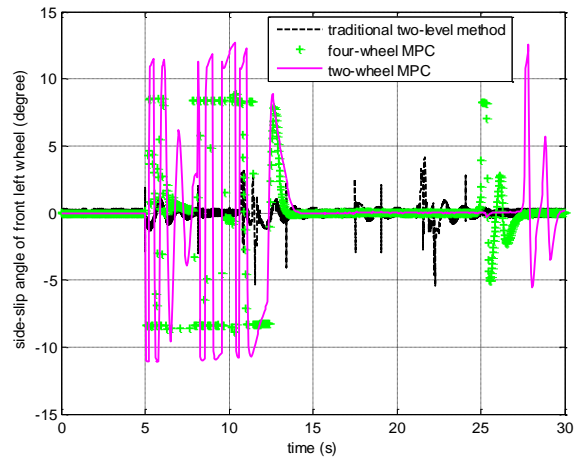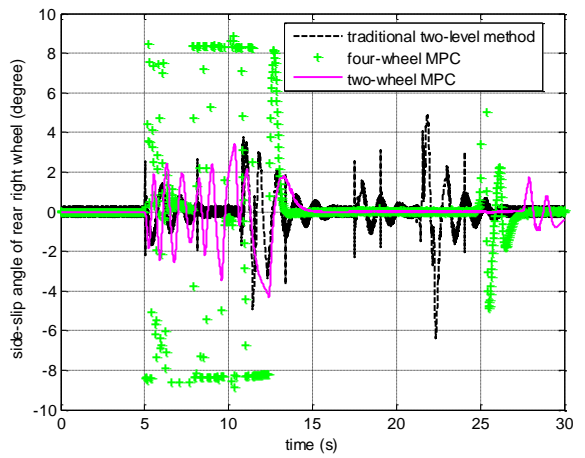


(a)



(b)

11

(c)

**Figure 6.** *Vehicle dynamics response in the second set of simulations.*

**(a)** longitudinal velocity **(b)** yaw rate **(c)** body side-slip angle
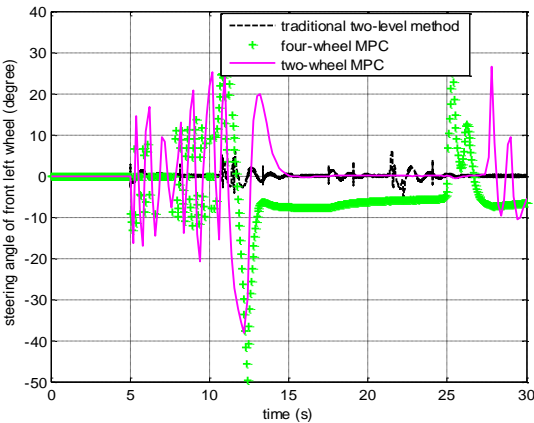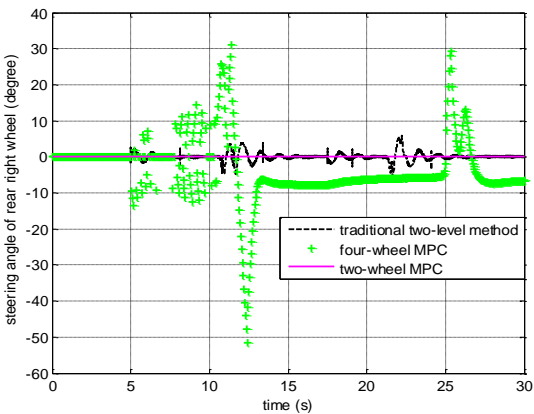


(a)



(b)



(c)



(d)

**Figure 7.** *Vehicle steering angle and side-slip angle responses in the second set of simulations.*

**(a)** steering angle of front left wheel **(b)** steering angle of rear right wheel **(c)** side-slip angle of front left wheel **(d)** side-slip angle of rear right wheel
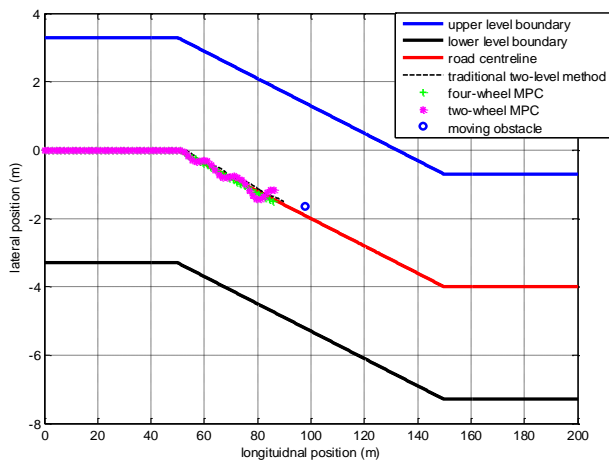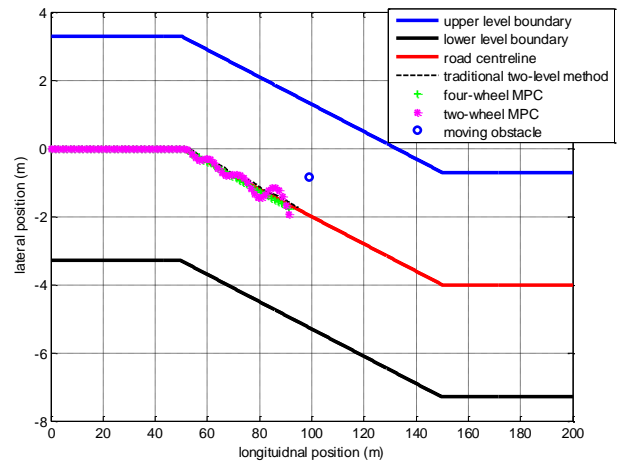
In the third set of simulations, the autonomous vehicle is still implementing the single lane change task with the same boundary condition in Figure 3. The initial longitudinal velocity of ego vehicle is still 10 m/s. The obstacle is assumed to move randomly to present the moving obstacles, which is different from the static obstacles in the second set of simulations. The heading angle and longitudinal acceleration of the moving obstacle is assumed as the random values with normal distribution (For the heading angle, mean value is 0 and variance is 10; for the longitudinal acceleration, mean value is 0 and the variance 40). In order to test the robustness of the proposed MPC method under changing tyre road friction coefficient, it is assumed the tyre road friction coefficient changes from 0.9 into 0.5 at 5 seconds, and then

changes back to 0.9 at 12 seconds. Figure 8 (a-d) presents the trajectory of the autonomous vehicle controlled by various control strategies at 9 seconds, 9.5 seconds, 10.5 seconds and 11.5 seconds. The proposed MP algorithm based on four-wheel model and two-wheel model can successfully carry out the obstacle avoidance manoeuvre. However, since it is hard to determine the boundary point of moving obstacle and applied the proposed two-point repulsive potential method, the proposed four-wheel MPC and two-wheel MPC method may not maintain the safety distance between the ego vehicle and the moving obstacle. The traditional two-level method cannot generate the avoidance trajectory although the repulsive potential of the moving obstacle has been included in the optimization cost function of two-level method. Figure 9(a) shows that the yaw rate of four-wheel based method is smaller than the two-wheel based method. Figure 9(b) suggests that the body side-slip angle response of the four-wheel model based method is larger since more control effort is applied to improve the trajectory control and yaw rate control performance. Similar to Figure 7, it can be seen form Figure 10 that all the proposed method satisfy both the constraints of individual wheel steering angle and side-slip angle.
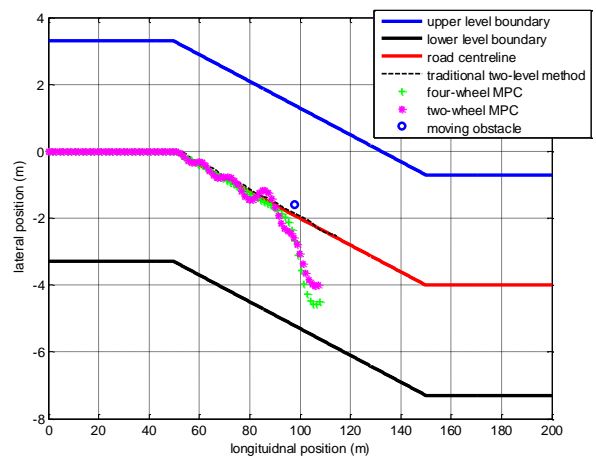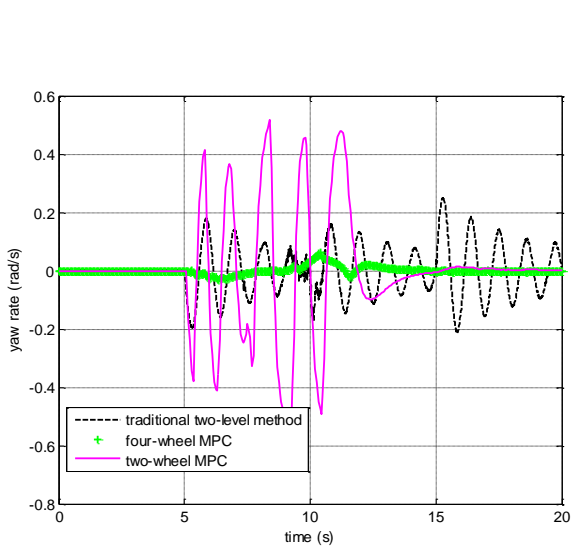


(b)



(c)
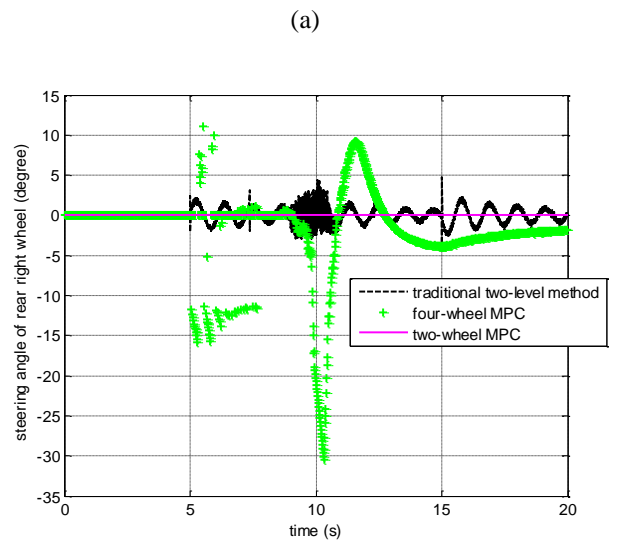


(d)



(a)
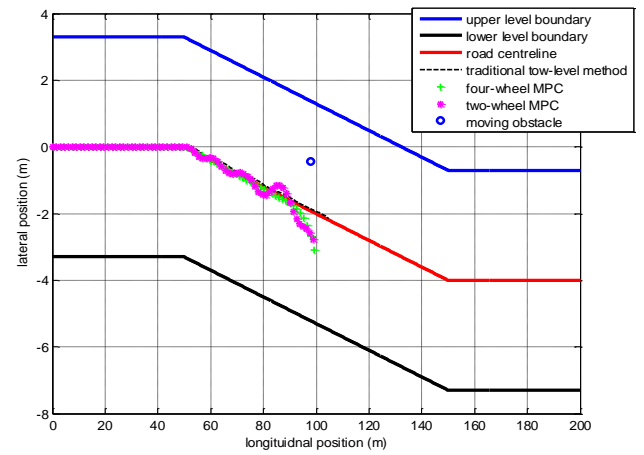
**Figure 8.** *Vehicle desired and actual trajectory in the third set of simulations.*
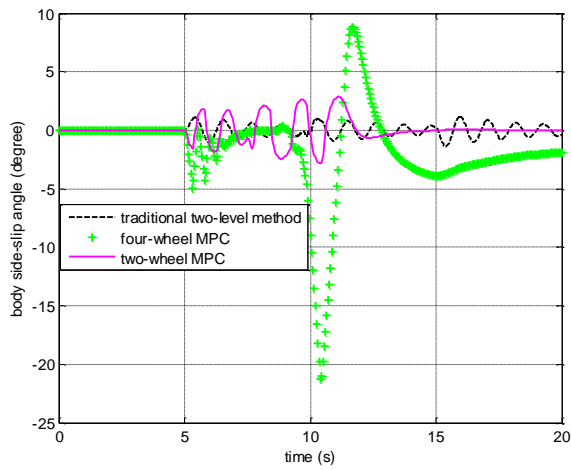
(a) at 9 seconds (b) at 9.5 seconds (c) at 10.5 seconds (d) at 11.5 seconds
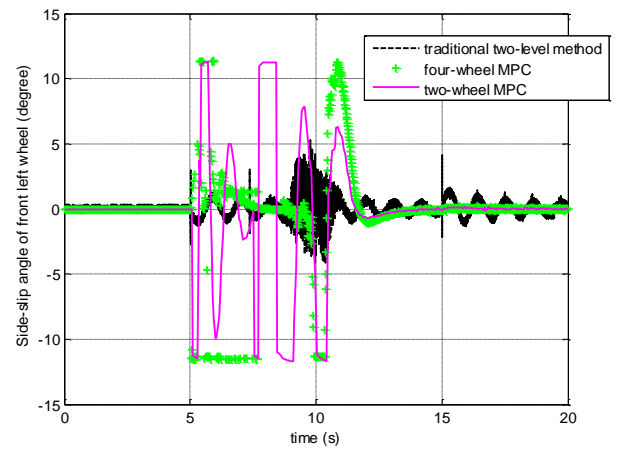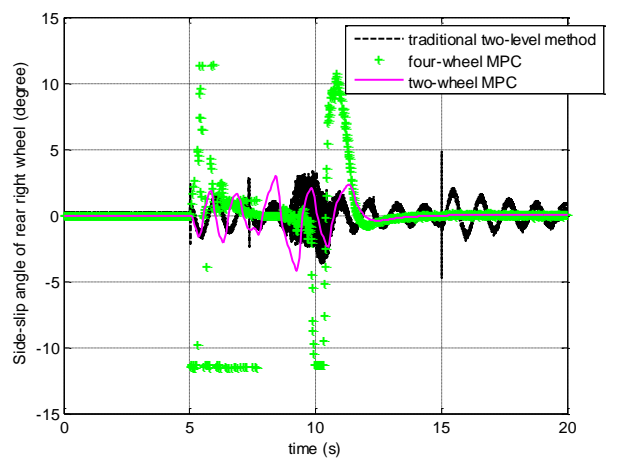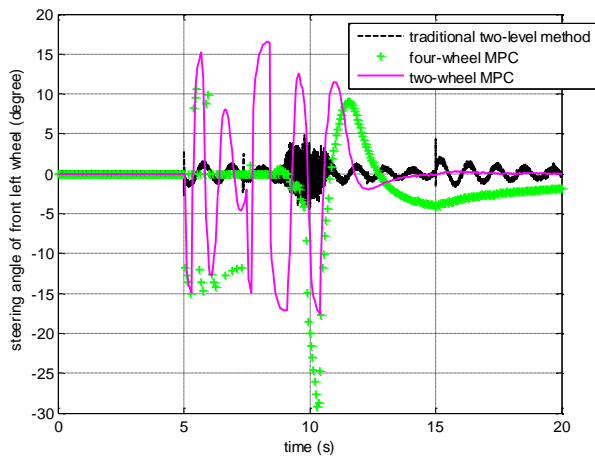
(a)



(b)



(b)

*Figure 9. Vehicle dynamics response in the third set of simulations.*

(a) yaw rate (b) body side-slip angle



(c)





(d)

*Figure 10. Vehicle steering angle and side-slip angle responses in the third set of simulations.*

(a) steering angle of front left wheel (b) steering angle of rear right wheel (c) side-slip angle of front left wheel (d) side-slip angle of rear right wheel

In Table 3, the actual computational time of the traditional two-level method, two-wheel MPC method and four-wheel MPC method in all the three sets of simulations are compared. It can be concluded that the proposed MPC method in general is much more computational efficient than the traditional two-level method. Due to the complex four-wheel model in the MP algorithm, the proposed four-wheel MPC is more time-consuming than the two-wheel MPC in certain scenario. It is noted that the actual time spent in the simulation environment of Matlab is quite large since the major disadvantage of the Matlab language is very time-consuming during the implementation. Thus, Matlab language only suits for the computer simulation for the research purpose and can be hardly applied on the actual autonomous vehicle control system. When the proposed method is implemented on the autonomous vehicle, the more computational efficiency programming language (such as C or C++) should be utilised for the coding of the proposed MP algorithm to meet the real-time trajectory control requirement.

**Table 3.** The actual time spent on each set of simulations (unit: second)

| Simulation number | Simulation time | Traditional two-level method | Two-wheel MPC | Four-wheel MPC |
|---|---|---|---|---|
| 1 | 20 | 1226 | 108 | 131 |
| 2 | 30 | 927 | 170 | 314 |
| 3 | 20 | 1822 | 108 | 160 |

## 7. Conclusion

This study proposes an innovative real-time integrated trajectory planning and control method based on the MP algorithm for a 4WIS-4WID electric vehicle. The four-wheel dynamics model and nonlinear Dugoff tyre model are applied in the proposed integrated control method to better present the tyre non-linear characteristic and fully utilise the advantages of 4WIS-4WID vehicle. The major findings of the simulation results can be summarised as the followings:

1) The trajectory planning and trajectory control can be successfully integrated in the MP optimisation algorithm in the real-time without the application of the trajectory tracking controller.

2) The proposed MP algorithm based on four-wheel model can fully utilise the advantage of the 4WIS-4WID

vehicle, and four steering wheels and four driving torques can be independently controlled.

3) The proposed MP algorithm based on four-wheel model can generate smoother trajectory with smaller yaw angle change rate compared with the MP algorithm based on two-wheel model.

4) The proposed MP method shows robustness control performance at different longitudinal velocities and different tyre-road friction coefficients.

5) The proposed integrated method based on MP algorithm can significantly improve the computational efficiency compare with the traditional two-level method which separates the trajectory planning and trajectory tracking control.

6) For the static obstacle, the simulations results prove that the proposed MP method can successfully avoid the obstacle by applying the two-point repulsive potential method. For the moving obstacle, the simulation results also verify that the proposed method can successfully generate the obstacle avoidance trajectory.

In the future, instead of the study on the trajectory planning and control of single autonomous vehicle, we will focus on the interaction between the vehicles nearby and propose the trajectory control of multiple on-road autonomous vehicles.

## 8. Acknowledgments

## 9. References

[1] Falcone, P., Borrelli, F., Asgari, J., Tseng, H., Hrovat, D.,: 'A real-time model predictive control approach for autonomous active steering', in In IFAC workshop on NMPC for fast systems, Grenoble, France, 2006.

[2] Falcone, P., Borrelli, F., Asgari, J., Tseng, H., Hrovat, D.,: 'Predictive active steering control for autonomous vehicle systems', IEEE Transactions on Control Systems Technology, 2007, 15, (3), pp. 566-580.

[3] Schorn, M.,: 'Quer-und Langsregelung eines Personenkraftwagens furein Fahrerassistenzsystem zur Unfallvermeidung', Ph.D. dissertation,Technische Universit¨at Darmstadt, 2007.

15

[4] Katriniok, A.,: 'Optimal vehicle dynamics control and state estimation for a low-cost GNSS-based collision avoidance system', VDI-Verlag, Dusseldorf, 2013.

[5] Qin, S., Badgwell, T.,: 'A survey of industrial model predictive control technology', Control Engineering Practice, 2003, 11, (7), pp. 732-764.

[6] Kim, H., Shim, D.,: 'A flight control system for aerial robots: Algorithms and experiments', Control Engineering Practice, 2003, 11, (12), pp. 1389-1400.

[7] Kim, H., Shim, D., Sastry, S.,: 'Nonlinear model predictive tracking control for rotorcraft-base unmanned aerial vehicles', in Proceedings of the American control conference, Anchorage, AK, 2002, pp. 3576-3581.

[8] Borrelli, F., Bemporad, A., Fodor, M., D. Hrovat,: 'An MPC/hybrid system approach to traction control', IEEE Trans. Control Systems Technology, 2006, 14, (3), pp. 541-552.

[9] Diehl, M., Bock, H., Schloder, J., Findeisen, R., Nagy, Z., Allgower, F.,: 'Real-time optimization and nonlinear model predictive control of processes governed by differential-algebraic equations', J.Proc. Contr, 2002, 12, (4), pp. 577-585.

[10] Keller, M., Hass, C., Seewald, A., Bertram, T., 'A model predictive approach to emergency maneuvers in critical traffic situations', in International IEEE Conference on Intelligent Transportation Systems, Spain, 2015, pp. 369-374.

[11] Ziegler, J., Bender, P., Dang, T., Stiller, C.,: 'Trajectory planning for bertha 2014; a local, continuous method', in International IEEE Conference on Intelligent Vehicles Symposium, Dearborn, MI, USA, 2014, pp. 450-457.

[12] Rosolia, U., Bruyne, S., Alleyne, A.,: 'Autonomous vehicle control: a nonconvex approach for obstacle avoidance', IEEE Transactions on Control System Technology, 2017, 25, (2), pp. 469-484.

[13] Yoon, Y., Shin, J., Kim, H., Park, Y., Sastry, S.,: 'Model-predictive active steering and obstacle avoidance for autonomous ground vehicles', Control Engineering Practice, 2009, 17, pp. 741-750.

[14] Liu, J., Jayakumar, P., Stein, J.L., Ersal, T.,: 'A multi-stage optimisation formulation for MPC-based obstacle avoidance in autonomous vehicles using a LIDAR sensor', in Proceedings of the ASME 2014 Dynamic Systems and Control Conference, San Antonio, TX, USA, 2014.

[15] Frasch, J.V., Gray, A., Zanon, M., Ferreau, H.J., Sager, S., Borrelli, F., Diehl, M.,: 'An auto-generated nonlinear MPC algorithm for real-time obstacle', in 2013 European Control Conference (ECC), Zürich, Switzerland, 2013, pp. 4136-4141.

[16] Gray, A., Gao, Y., Lin, T., Hedrick, J., Tseng, E, Borrelli, F.,: 'Predictive control for agile semi-autonomous ground vehicles using motion primitves', in Proceedings American Control Conference, Montréal, Canada, 2012, pp. 4239-4244.

[17] Gao, Y., Lin, T., Borrelli, F., Tseng, E., Hrovat, D.,: 'Predictive control of autonomous ground vehicles with obstacle avoidance on slippery road', in Dynamic Systems and Control Conference, Massachusetts, USA, 2010.

[18] Li, B., Li, W., Kennedy, O., Du, H.,: 'The dynamics analysis of an omni-directional vehicle', International Journal of Automotive Technology, 2014, 15, (3), pp. 387-398.

[19] Boada, B., Boada, M., Díaz, V.,: 'Fuzzy-logic applied to yaw moment control for vehicle stability', Vehicle System Dynamics, 2005, 43, (10), pp. 753-770.

[20] Dugoff, H., Fancher, P., Segel, L.,: 'An analysis of tyre traction properties and their influence on vehicle dynamic performance', SAE 700377, 1970, pp. 1219-1243.

[21] Zhao, Y., Zhang, J.,: 'Yaw stability control of a four-independent-wheel drive electric vehicle', Int. J. Electric and Hybrid Vehicles, 2009, 2, (1), pp. 64-76.

[22] Wang, J., Alexander, L., Rajamani, R.,: 'Friction estimation on high-way vehicles using longitudinal measurements', ASME J. Dyn. Syst.,Meas. Control, 2004, 126, (2), pp. 265-275.

[23] Rajamani, R., Phanomchoeng, G., Piyabongkarn, D., Lew, J.,: 'Algorithms for real-time estimation of individual wheel tire-road friction coefficients', IEEE/ASME Transactions on Mechatronics, 17, (6), pp. 1183-1195, 2012.

[24] Li, B., Du, H., Li, W.,: 'Comparative study of vehicle tyre–road friction coefficient estimation with a novel cost-effective method', Vehicle System Dynamics, 2014, 52, (8), pp. 1066-1098.

[25] Li, B., Du, H., Li, W.,: 'Potential field approach-based trajectory control for autonomous electric vehicles with in-wheel motors', IEEE Transactions on Intelligent Transportation System, 2017, 18, (8), pp. 2044-2055.

[26] Lam, T., Qian, H., Xu, Y.,: 'Omnidirectional Steering Interface and Control for a Four-Wheel Independent Steering Vehicle', IEEE/ASME Transactions on Mechatronics, 2010, 15, (3), pp. 329-338.

[27] Chen, Y., Wang, J.,: 'Design and experimental evaluations on energy efficient control allocation methods for overactuated electric vehicles: Longitudinal motion case', IEEE Transactions on Mechatronics, 2014, 19, (2), pp. 538-548.

[28] Hata, A., Wolf, D.,: 'Feature decision for vehicle localization in urban environments using a multilayer LIDAR', IEEE Transcations on Intelligent Transportation System, 2016, 17, (2), pp. 420-429.

[29] Dickmann, J.,: 'Radar contribuition to highly automated driving', in 44th European Microwave Conference (EuMC), Rome, Italy, 2014, pp. 1715-1718.

[30] Broggi, A.,: 'Terramax vision at the urban challenge 2007', IEEE Transaction on Intelligent Transportation System, 2010, 11, (1), pp. 194-205.

[31] Chavez-Garcia, R., Aycard, O.,: 'Multiple sensor fusion and classification for moving object detection and tracking', 2016, IEEE Transaction on Intelligent Transportation System, 17, (2), pp. 525-534.

[32] Schaub, A., Baumgartner, D., and Burschka, D.,: 'Reactive obstacle avoidance for highly maneuverable vehicles based on a two-stage optical flow clustering', IEEE Transcations on Intelligent Transportation System, 2017, 18, (8), pp. 2137-2152.

[33] Lin, C., Juang, J., Li, K.,: 'Active collision avoidance system for steering control of autonomous vehicles', IET Intelligent Transport Systems, 2014, 8, (6), pp. 550-557.